Progress In Electromagnetics Research Letters, Vol. 110, 109–116, 2023

Frequency Diverse Arc Array Beampattern Synthesis Analysis with Nonlinear Frequency Offset

Zhuo Deng[1, 2, *], Wei Xu[1, 2], Pingping Huang[1, 2], Weixian Tan[1, 2], and Yaolong Qi[1, 2]

Abstract—Frequency diversity array (FDA) can generate range and angle dependent "S" beam patterns, but there is a problem of range and angle coupling, which can be well solved by using nonlinear frequency offset in recent years' research. The rotational symmetry of the arc-shaped structure brings the beam scanning capability of the array antenna within a range of 360°, which can realize the all-round monitoring of the target position, and provides a more flexible method for radar communication. In this paper, a nonlinear frequency offset based frequency diversity arc array (FDAA) beam scanning method is proposed, which activates the selection matrix according to the target direction. In order to form equal phase plane beam scanning, phase compensation between array elements is carried out, and three kinds of nonlinear frequency bias are introduced to simulate beampattern synthesis. Compared with the traditional linear frequency offset FDAA, the numerical simulation results verify the feasibility and effectiveness of the scheme.

1. INTRODUCTION

The concept of non-traditional array antennas such as frequency diversity array (FDA) was proposed by Antonik et al. in 2006 [1]. Compared with the traditional phased array radar [2], there is a small frequency offset between the antenna elements [3], so that the phase superposition relationship of the transmitted signal in the far field changes with the change of the target range, and it forms a beam pattern related to range, angle, and time [4], which can distinguish the clutter interference of the target in the range dimension. It has broad application prospects in target location [5, 6], interference suppression [7, 8], and other fields.

FDA has attracted more and more attention because of its unique range and angular spatial focusing characteristics [9, 10]. In terms of FDA point beam optimization, [11] uses nonlinear array element spacing to break the periodicity of the FDA. [12] uses a logarithmically increased frequency offset to remove the range-angle coupling of the FDA beampattern. Using quadratic and cubic power functions to increase the frequency offset to focus the transmitted energy [13], compared with the logarithmic frequency offset, its performance in the range dimension is greatly improved. In [14], a symmetrical multi-carrier frequency control array based on convex optimization is proposed, which forms a "dot-shaped" beam pattern and improves the performance of energy focusing and side lobe suppression. Through the design of a new type of functional frequency offset [15] combining natural logarithm and sin function and the proposed Hamming window function frequency offset [16], the results of these two methods are superior to logarithmic frequency bias and other functional frequency bias. Then, methods such as symmetric logarithmic frequency offset [17], discrete Fourier transform [18], and Taylor window function [19] have also achieved good results in suppressing sidelobes in the range domain and angle domain, and obtained a superior spot beam pattern. In terms of FDA beam interference suppression,

Received 2 March 2023, Accepted 18 April 2023, Scheduled 25 May 2023

* Corresponding author: Zhuo Deng (dengz20@163.com).

[1] College of Information Engineering, Inner Mongolia University of Technology, Hohhot, China. [2] Inner Mongolia Key Laboratory of Radar Technology and Application, Hohhot, China.

the combination of FDA and multiple-input multiple-output (MIMO) systems can produce the ability to suppress interference in different scenarios [20]. The Chebyshev window function is used to calculate the transmit weight coefficient and frequency offset increment coefficient [21], which realizes the low side lobe of the target beam. A multi-carrier nonlinear frequency modulation system based on pseudo-random frequency offset is proposed in [22], which can reduce the main lobe width and side lobe level, and also simplifies the radar system.

Considering the single linear structure of the traditional frequency control array, its beam scanning has certain angle limitations. Under extreme angle conditions, the antenna gain will decrease [23], and the main lobe beam will be widened, which is not conducive to target monitoring. For the application scenarios that require antennas to scan in all directions in various fields, [24–26] have conducted research on the design of antenna structures. The circular geometry is worthy of the use of antenna beamforming and application geometry [27–29]. In this paper, we propose a frequency diverse arc array (FDAA) that achieves 360° omnidirectional beam scanning capability by selecting active array elements and precise phase compensation. By applying additional nonlinear frequency bias to each array element, the method of controlling the beam orientation pattern in the target range domain and angle domain is provided, and the selected target region can be comprehensively monitored in the 360° range, which makes the target region locking more accurate and reliable.

The rest of the letter is organized as follows. Section 2 expounds the geometric model and working element selection method with FDAA. Section 3 constructs the phase compensation of the array elements on the equiphase plane, introduces three kinds of nonlinear frequency offset functions, and proposes the FDAA antenna beamforming method based on the nonlinear frequency offset. Section 4 compares and analyses the experimental results of three nonlinear frequency offset FDAA beams. Finally, the conclusion is drawn in Section 5.

2. FDAA STRUCTURE ANALYSIS

2.1. Antenna Geometric Model

FDAA adopts an open horn-shaped directed array element with one type of transmitting and receiving. As shown in Fig. 1, a series of antenna array elements are evenly distributed along the angle direction of the circular arc to form FDAA. The total number of array elements inside the whole ring is N; the array radius is R; the angle interval of adjacent arrays on the ring is $\Delta\phi$; and the spacing between adjacent arrays on the ring is d_c. The aperture angle composed by activating the selected working element is ϕ.

In order to analyze the structure of FDAA more deeply, as shown in Fig. 2, taking the true north direction as the reference direction, it is assumed that the angle θ of point P of the far-field target is

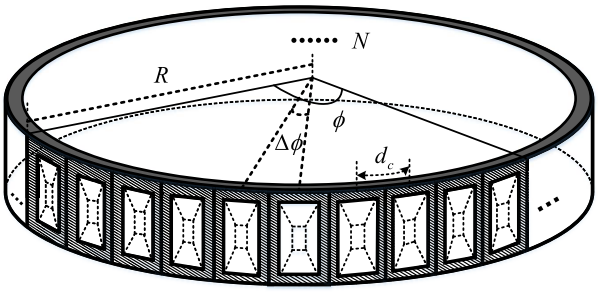

Figure 1. The FDAA 3D model diagram.

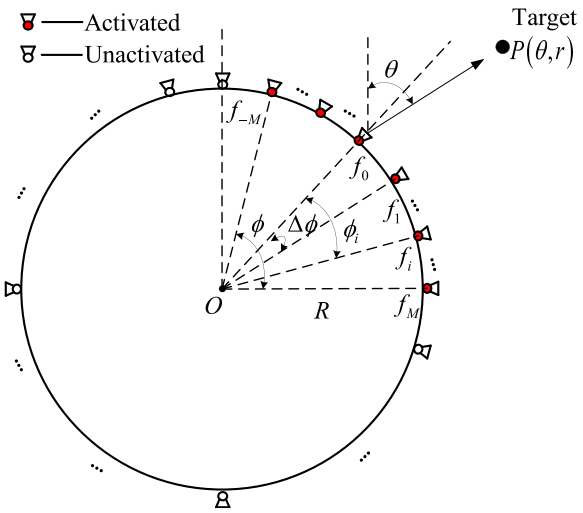

Figure 2. Structural analysis of FDAA.

the angle between the target direction and the true north direction, and the range of θ is $[0, 360^\circ)$. Set the antenna element with the beam pointing to the true north as the 0th array element, number the N array elements in the circle clockwise, and add an additional frequency offset between the array elements, then, the method of selecting element f_0 in the true north direction as the reference element is as follows:

$$f_0 = \text{round}\left(\frac{\theta}{\Delta\phi}\right) = \text{round}\left(\frac{\theta}{360/N}\right) \tag{1}$$

Among them, round $(\cdot)$ represents the rounding operation, and $\Delta\phi$ represents the included angle between adjacent arrays, which can also be called beam hop.

2.2. Activated Element Selection Method

Due to the special curvature effect of FDAA, the nonlinear distribution of spatial phase difference is caused. As the array main beam direction deviates from the maximum radiation direction, angle of the array element increases; the radiation field intensity of the array element will decrease accordingly; and a single array element can only contribute to the gain of the array main beam in a certain region. Therefore, it is necessary to activate the appropriate array to form the working array under different scanning angles and use the feed system to select and activate the working array accordingly. According to the relationship between the horizontal length L of the working array formed by the activated array and the maximum beam width θ_{BW} of the far-field target P in the angle domain:

$$L = k \cdot \frac{\lambda}{\theta_{BW}} \tag{2}$$

where k is the 3 dB beam width coefficient; k is usually one of the coefficients in $(0.88, 1.2)$; and λ is the wavelength. It can be concluded that the aperture angle composed by the active array is:

$$\phi = 2\arcsin\left(\frac{kc}{2Rf_c\,\theta_{BW}}\right) \tag{3}$$

where c is the speed of light, and f_c is the carrier frequency. According to the geometric relationship of the arc structure, the total number of activated arrays can be expressed as:

$$N_A = 2 \cdot \left\lfloor \frac{\phi}{2 \cdot \Delta\phi} \right\rfloor + 1 \tag{4}$$

where $\lfloor\cdot\rfloor$ represents the integer operation, as shown in Fig. 1, $N_A = 2M + 1$.

3. FDAA BEAMPATTERN SYNTHESIS

3.1. Phase Compensation

Due to the special curved surface structure of FDAA, it is necessary to calculate the phase compensation of the equiphase plane when scanning the beam in the target azimuth direction. As shown in Fig. 3, with array element f_0 as the central reference array element, the spatial range difference between the effective working array element and the central reference array element can be expressed as:

$$D_m = R \cdot (1 - \cos\phi_m) \tag{5}$$

Then, the spatial phase difference between each effective array element and the central reference array element can be expressed, that is, the required phase compensation to form the isophase plane:

$$\Delta\varphi_m = \frac{2\pi f_c}{c} \cdot D_m \tag{6}$$

where f_c is the frequency of the central reference array element, c the speed of light, and R the radius of the FDAA antenna. ϕ_m is the central angle between the mth array element and the central reference array element.

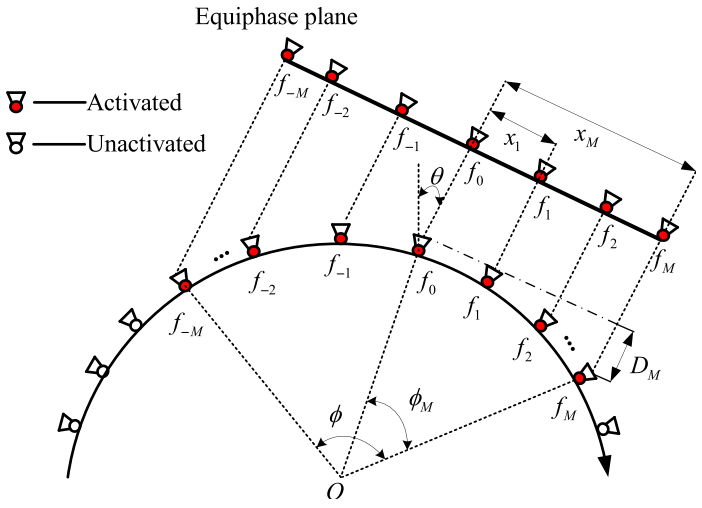

Figure 3. Phase compensation of working element.

3.2. Frequency Design

Under the influence of the FDAA structure, a symmetrical frequency offset needs to be designed according to the position of the central reference array element to achieve precise focusing on a single maximum beampattern. The equalphase surface shown in Fig. 3 is composed of m activated working array elements, which have the characteristics of nonuniform spacing. The frequency of the transmitted signal of the mth array element is designed as:

$$f_m = f_c + \Delta f_m \tag{7}$$

where $m = -M, ..., 0, ..., M$, Δf_m is the frequency offset of the mth element, and Δf is a fixed frequency offset. The following three nonlinear frequency biases, Δf_{m1}, Δf_{m2} and Δf_{m3}, can be selected.

$$\Delta f_{m1} = \Delta f \cdot |\sin(m)| \tag{8}$$

$$\Delta f_{m2} = \Delta f \cdot \left[0.54 - 0.46\cos\left(\frac{2\pi\,|m|}{2M}\right)\right] \tag{9}$$

$$\Delta f_{m1} = \Delta f \cdot \ln\left(|m| + 1\right) \tag{10}$$

3.3. Beampattern Synthesis

As shown in Fig. 3, assuming that when the monitoring target is at point P, the monitoring target satisfies the far field approximation condition at any point, the signal emitted by the mth array can be written:

$$X_m\left(t\right) = \omega_m \exp\left(j2\pi f_m t\right), \quad 0 < t < T \tag{11}$$

where ω_m represents the complex weight of the mth element, and T represents the duration of the transmitted pulse. The range between the mth element and the target point should be:

$$r_m \approx r - x_m \sin\theta \approx r - R\sin\phi_m \sin\theta \tag{12}$$

where r is the range of the target; θ is the angle of the target; $f_0 \gg \Delta f_m$; $r \gg R\sin\phi_m \sin\theta$; then the total signal at the far-field monitoring target P point is:

$$\begin{aligned} X\left(t, r, \theta\right) &= \sum_{-(M-1)/2}^{(M-1)/2} X_m\left(t - \frac{r_m}{c}\right) \\ &\approx \exp\left[j2\pi f_c\left(t - \frac{r}{c}\right)\right] \sum_{-(M-1)/2}^{(M-1)/2} \omega_m \exp\left[j2\pi\Delta f_m\left(t - \frac{r}{c}\right)\right] \exp\left(j2\pi f_c \frac{R\sin\phi_m \sin\theta}{c}\right) \end{aligned} \tag{13}$$

In order to make the monitoring target get a single beam peak at (r_0, θ_0), we express the complex weight ω_m as:

$$\omega_m = \exp\left[j\left(\frac{2\pi\Delta f_m r_0}{c} - R\sin\phi_m \sin\theta_0 - \Delta\varphi_m\right)\right] \tag{14}$$

Finally, the FDAA beampattern expression with nonlinear frequency offset introduced is:

$$\begin{aligned} B\left(t, r_0, \theta_0\right) = & \left| \sum_{-(M-1)/2}^{(M-1)/2} \exp\left[j2\pi\Delta f_m\left(t - \frac{r - r_0}{c}\right)\right]\right. \\ & \left. \times \exp\left(j2\pi f_c \frac{R\sin\phi_m(\sin\theta - \sin\theta_0) - R\left(1 - \cos\phi_m\right)}{c}\right)\right|^2 \end{aligned} \tag{15}$$

4. SIMULATION RESULTS

The parameter settings in FDAA's antenna beampattern simulation experiment are shown in Table 1. Fig. 4 shows the FDAA with linearly increasing frequency offset. The designed linear frequency offset is $f(m) = |m| \cdot \Delta f$, and it can be seen that there are multiple peaks in the range domain and a large interference value in the angle domain. The target beampattern cannot form a single dot-shaped beampattern. To solve this problem, we designed the FDAA beam simulation diagram of the frequency offset of the sine function in Fig. 5(a), the frequency offset of the cosine function in Fig. 5(b), and the symmetrical logarithmic frequency offset in Fig. 5(c).

In Fig. 5(a), there are many interferences around the main lobe. The specific performance is that the side lobe level in the range domain is irregularly distributed, and the side lobe level in the angle domain is high, but the difference is not large. Overall, Table 2 shows the comparison of FDAA beampattern

Table 1. Simulation parameters.

Parameters	Symbol	Value
Carrier frequency	f_c	10 GHz
Frequency offset	Δf	30 kHz
Element number	M	33
Element spacing	d_c	$\lambda/2$
Array radius	R	0.3056 m
Array radian	ϕ	$\pi/2$
Target angle	θ_0	10°
Target angle	r_0	25 km

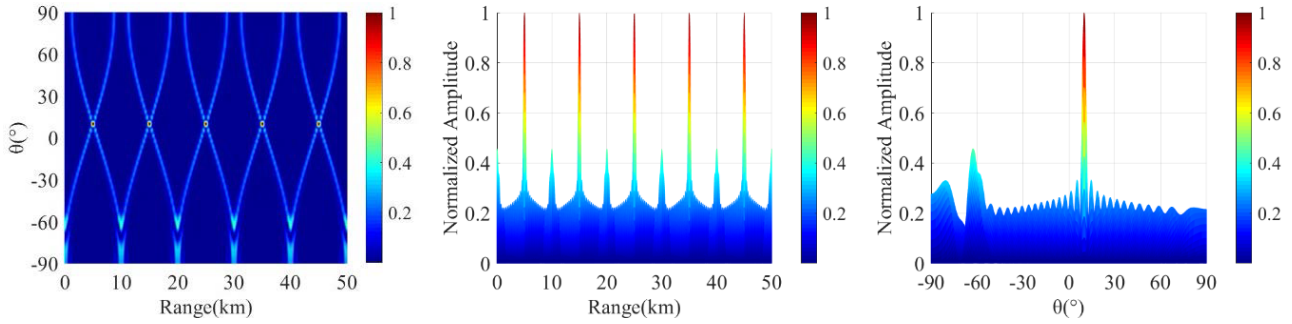

Figure 4. The FDAA with linear frequency offset.

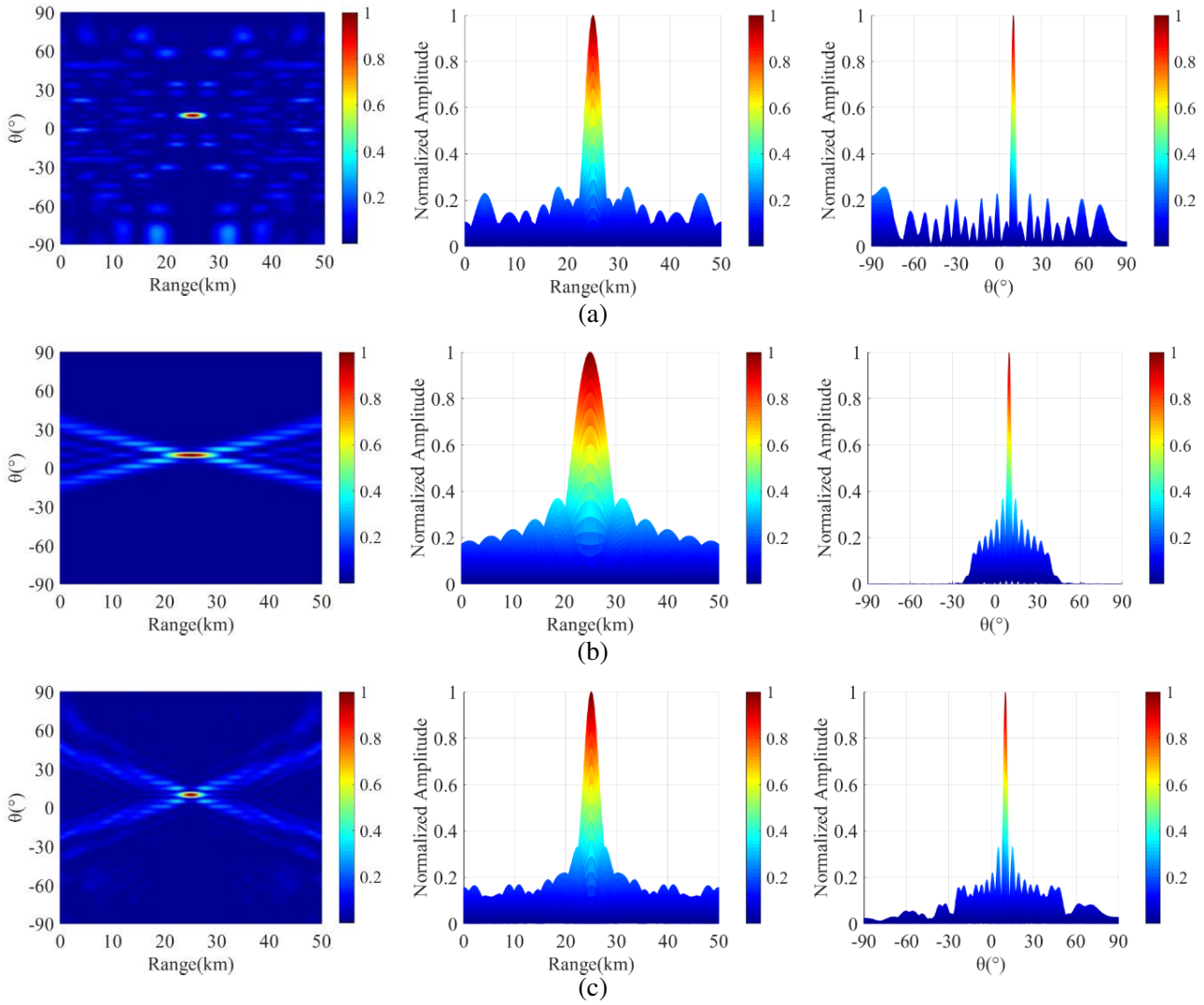

Figure 5. The FDAA with nonlinear frequency offset. (a) Sym-sin FDAA. (b) Hamming FDAA. (c) Sym-log FDAA.

Table 2. Comparison of FDAA beampattern performance based on different frequency offset.

Frequency offset scheme	3 dB beam width in range domain (m)	3 dB beam width in angle domain (°)	First sidelobe level
Linear frequency offset	$24.92 \sim 25.08$	$8.37 \sim 11.62$	0.45
Sym-sin frequency offset	$23.17 \sim 26.83$	$8.37 \sim 11.62$	0.26
Hamming frequency offset	$21.12 \sim 28.88$	$8.37 \sim 11.62$	0.36
Sym-log frequency offset	$23.07 \sim 26.93$	$8.37 \sim 11.62$	0.33

performances under different frequency offsets. The coupling between range and angle in Fig. 5(b) is completely removed. Compared with Fig. 5(a), the main lobe in the range domain is broadened, and the side lobes in the angle domain are more within $\pm 30°$ of the target. The only advantage is that the side lobes on both sides of the angle domain are basically 0. It can be clearly seen from Fig. 5(c) that the FDAA point beam has the best focusing effect; the main lobe width in the range domain is superior; and the level of the first side lobe is very low. The average is much lower than that in Fig. 5(b).

5. CONCLUSIONS

In this paper, FDAA, a new structure array antenna, is introduced to achieve 360-degree omni-directional beam scanning capability by selecting active array elements and phase compensation, which provides a new idea for radar, communication and target monitoring in specific real-world scenarios. A novel FDAA beampattern synthesis method based on nonlinear frequency offset is proposed, which is not restricted to the fixed orientation of the antenna for the scanning of the target point. The designed nonlinear frequency offset effectively solves the problem of range and angle coupling, reduces the interference of the sidelobe to the target, and obtains a better point beam and peak side lobe ratio. Numerical simulation results show that nonlinear frequency bias is a good choice for FDAA. In our subsequent work, we need to suppress the side lobe around the main lobe, enhance the radar antenna target location ability, and improve the measurement accuracy and resolution of the radar antenna.

ACKNOWLEDGMENT

This research was supported by the National Natural Science Foundation of China under Grant Number 62071258, 61971246 and 52064039, in part by Natural Science Foundation of Inner Mongolia, Grant Number 2020ZD18, in part by Key project of Regional Innovation and Development Joint Fund of National Natural Science Foundation under Grant Number U22A2010, and in part by Scientific Research Projects of University Directly of Inner Mongolia under Grant Number JY20220418.

REFERENCES

1. Antonik, P., M. C. Wicks, H. D. Griffiths, and C. J. Baker, "Frequency diverse array radars," *2006 IEEE Conference on Radar*, IEEE, Verona, NY, USA, 2006.
2. Wang, W. Q., "Frequency diverse array antenna: New opportunities," *IEEE Antennas and Propagation Magazine*, Vol. 57, No. 2, 145–152, 2015.
3. Ivashina, M. V., R. Maaskant, and B. Woestenburg, "Equivalent system representation to model the beam sensitivity of receiving antenna arrays," *IEEE Antennas and Wireless Propagation Letters*, Vol. 7, 733–737, 2008.
4. Wang, W. Q., "Range-angle dependent transmit beampattern synthesis for linear frequency diverse arrays," *IEEE Transactions on Antennas and Propagation*, Vol. 61, No. 8, 4073–4081, 2013.
5. Wang, Y., W. Q. Wang, and H. Chen, "Linear frequency diverse array manifold geometry and ambiguity analysis," *IEEE Sensors Journal*, Vol. 15, No. 2, 984–993, 2015.
6. Liao, T., Y. Pan, and W. Q. Wang, "Generalized linear frequency diverse array manifold curve analysis," *IEEE Signal Processing Letters*, Vol. 25, No. 6, 768–772, 2018.
7. Wang, Y. and S. Zhu, "Range ambiguous clutter suppression for FDA-MIMO forward looking airborne radar based on main lobe correction," *IEEE Transactions on Vehicular Technology*, Vol. 70, No. 3, 2032–2046, 2021.
8. Gui, R., W. Q. Wang, A. Farina, and H. C. So, "FDA radar with doppler-spreading consideration: Mainlobe clutter suppression for blind-doppler target detection," *Signal Processing*, Vol. 179, 107773, 2021.
9. Khan, W., I. M. Qureshi, A. Basit, A. N. Malik, and A. Umar, "Performance analysis of MIMO-frequency diverse array radar with variable logarithmic offsets," *Progress In Electromagnetics Research C*, Vol. 62, 23–34, 2016.
10. Nusenu, S. Y., H. Chen, W.-Q. Wang, S. Ji, and O. A. K. Opuni-Boachie, "Frequency diverse array using Butler matrix for secure wireless communications," *Progress In Electromagnetics Research M*, Vol. 63, 207–215, 2018.
11. Wang, W. Q., H. C. So, and H. Shao, "Nonuniform frequency diverse array for range-angle imaging of targets," *IEEE Sensors Journal*, Vol. 14, No. 8, 2469–2476, 2014.

12. Khan, W., I. M. Qureshi, and S. Saeed, "Frequency diverse array radar with logarithmically increasing frequency offset," *IEEE Antennas and Wireless Propagation Letters*, Vol. 14, 499–502, 2015.
13. Gao, K., W. Q. Wang, J. Cai, and X. Jie, "Decoupled frequency diverse array range-angle-dependent beampattern synthesis using non-linearly increasing frequency offsets," *IET Microwaves, Antennas & Propagation*, Vol. 10, No. 8, 880–884, 2016.
14. Shao, H., J. Dai, J. Xiong, H. Chen, and W. Q. Wang, "Dot-shaped range-angle beampattern synthesis for frequency diverse array," *IEEE Antennas and Wireless Propagation Letters*, Vol. 15, 1703–1706, 2016.
15. Chen, B., X. Chen, Y. Huang, and J. Guan, "Transmit beampattern synthesis for the FDA radar," *IEEE Antennas and Wireless Propagation Letters*, Vol. 17, No. 1, 98–101, 2018.
16. Basit, A., I. M. Qureshi, W. Khan, S. U. Rehman, and M. M. Khan, "Beam pattern synthesis for an FDA radar with hamming window-based nonuniform frequency offset," *IEEE Antennas and Wireless Propagation Letters*, Vol. 16, 2283–2286, 2017.
17. Liao, Y., W. Q. Wang, and Z. Zheng, "Frequency diverse array beampattern synthesis using symmetrical logarithmic frequency offsets for target indication," *IEEE Transactions on Antennas and Propagation*, Vol. 67, No. 5, 3505–3509, 2019.
18. Zubair, M., S. Ahmed, and M. S. Alouini, "Frequency diverse array radar: New results and discrete fourier transform based beampattern," *IEEE Transactions on Signal Processing*, Vol. 68, 2670–2681, 2020.
19. Liao, Y., H. Tang, X. Chen, and W. Q. Wang, "Frequency diverse array beampattern synthesis with Taylor windowed frequency offsets," *IEEE Antennas and Wireless Propagation Letters*, Vol. 19, No. 11, 1901–1905, 2020.
20. Wang, W. Q. and H. C. So, "Transmit subaperturing for range and angle estimation in frequency diverse array radar," *IEEE Transactions on Signal Processing*, Vol. 62, No. 8, 2000–2011, 2014.
21. Nusenu, S. Y., A. Basit, and E. Asare, "FDA transmit beamforming synthesis using Chebyshev window function technique to counteract deceptive electronic countermeasures signals," *Progress In Electromagnetics Research Letters*, Vol. 90, 53–60, 2020.
22. Wang, Z., T. Mu, Y. Song, and Z. Ahmad, "Beamforming of frequency diverse array radar with nonlinear frequency offset based on logistic map," *Progress In Electromagnetics Research M*, Vol. 64, 55–63, 2018.
23. Xu, W., J. Hu, P. Huang, W. Tan, and Y. Dong, "Multiaperture antenna architecture design for azimuth uniform sampling in high-resolution wide-swath SAR," *IEEE Antennas and Wireless Propagation Letters*, Vol. 19, No. 6, 1042–1046, 2020.
24. Donelli, M., T. Moriyama, and M. Manekiya, "A compact switched-beam planar antenna array for wireless sensors operating at Wi-Fi band," *Progress In Electromagnetics Research C*, Vol. 83, 137–145, 2018.
25. Donelli, M. and P. Febvre, "An inexpensive reconfigurable planar array for Wi-Fi applications," *Progress In Electromagnetics Research C*, Vol. 28, 71–81, 2012.
26. Viani, F., L. Lizzi, M. Donelli, D. Pregnolato, G. Oliveri, and A. Massa, "Exploitation of parasitic smart antennas in wireless sensor networks," *Journal of Electromagnetic Waves and Applications*, Vol. 24, No. 7, 993–1003, 2010.
27. Lin, Y., W. Hong, W. Tan, Y. Wang, and M. Xiang, "Airborne circular SAR imaging: Results at P-band," *2012 IEEE International Geoscience and Remote Sensing Symposium*, 5594–5597, 2012.
28. Huang, P., W. Tan, and Y. Su, "MIMO-SAR imaging technology for helicopter-borne based on ARC antenna array," *2015 IEEE International Geoscience and Remote Sensing Symposium (IGARSS)*, 1801–1804, 2015.
29. Akkoc, A., E. Afacan, and E. Yazgan, "Dot-shaped 3D range-angle dependent beamforming with discular frequency diverse array," *IEEE Transactions on Antennas and Propagation*, Vol. 69, No. 10, 6500–6508, 2021.